Journal of Photochemistry and Photobiology A: Chemistry 201 (2009) 214–221

Contents lists available at ScienceDirect

Journal of Photochemistry and Photobiology A: Chemistry

journal homepage: www.elsevier.com/locate/jphotochem

Terbium(III)-containing organic–inorganic hybrids synthesized through hydrochloric acid catalysis

P.P. Lima [a,*], R.A.S. Ferreira [a], S.A. Júnior [b], O.L. Malta [b], L.D. Carlos [a]

[a] Department of Physics, CICECO, University of Aveiro, 3810-193 Aveiro, Portugal
[b] Departamento de Química Fundamental, CCEN – UFPE, Cidade Universitária, 50670-901 Recife, PE, Brazil

ARTICLE INFO

Article history:
Received 14 September 2008
Received in revised form 22 October 2008
Accepted 24 October 2008
Available online 13 November 2008

Keywords:
Di-ureasils
Acid-catalysis
Lanthanide complex
Photoluminescence
Emission quantum yield

ABSTRACT

Organic–inorganic hybrids incorporating $Tb(acac)_3{\cdot}3H_2O$ (where acac is acetylacetonate) were synthesized via conventional hydrolysis sol–gel reaction in the presence and absence of an acid catalyst (hydrochloric acid, HCl). The host framework of these materials, named di-ureasils, is formed by polyether-based chains grafted to both ends to a siliceous backbone through urea cross-linkages (–NHC(C=O)NH–). Four different concentrations of HCl (0.5, 1.0, 1.5, and 2.0 mol L^{-1}) were used as catalyst for hydrolysis reactions. The gelation time of the resulting materials depends on the HCl concentration varying between 5 and 20 min. The hybrids were characterized by X-ray diffraction (XRD), Fourier transform infrared spectroscopy (FTIR), ^{29}Si and ^{13}C magic-angle spin nuclear magnetic resonance (NMR) and photoluminescence spectroscopy. The emission quantum yield for the undoped hybrids lies between 8.7 and 10.6%, much higher than those obtained for analogous samples prepared via conventional hydrolysis in the absence of catalyst. For the Tb^{3+}-containing hybrids the lanthanide local environment was affected due to different synthetic conditions used. An increase in the $^5D_4$ lifetime values, relatively to that of the isolated $Tb(acac)_3{\cdot}3H_2O$ complex, is in good agreement with a smaller $^5D_4$ non-radiative transition probability in the hybrids suggesting the replacement of the Tb^{3+}coordinated water molecules by the oxygen atom of the carbonyl group of the di-ureasil host.

1. Introduction

In recent years there has been an increasing interest in the optical properties of lanthanide complexes due to their large range of applications, such as organic light-emitting diodes (OLEDs) [1–5], luminescent sensors [6,7] and UV dosimeters [8,9]. Particularly, the lanthanide β-diketonate complexes have been extensively investigated essentially because their efficient light emission under UV excitation [10,11], despite they are generally obtained with two or three water molecules in the first coordination sphere that quench the luminescence. Moreover, the poor thermal and mechanical stability of lanthanide β-diketonate complexes do not permit their use in tunable solid-state laser or phosphor devices. In order to circumvent these shortcomings, neutral ligands, such as 2,2-bipyridine [12] and dimethyl sulphoxide (DMSO) [13], have been used to replace the water molecules in the first coordination sphere and the complexes have been incorporated into polymer [14–16] and organic–inorganic hybrid hosts [17–20].

The sol–gel method [21,22] is a promising technique for the development of organic–inorganic hybrids with technological interest for optics and photonics due to the following advantages: mild reaction conditions, processing versatility, possibility of mixing the organic and inorganic precursor components at the nanometer scale, and ability of tailoring the final properties of the material through adequate choice of the organic and inorganic components [23,24]. Among the organic–inorganic hybrid hosts reported in the last two decades, of particular interest are the luminescent di-ureasils whose hybrid framework consists of a siliceous skeleton grafted to poly(ethylene oxide) chains through urea cross-linkages [25]. In these materials the white-light photoluminescence results from a convolution of donor–acceptor pair recombinations that occur in the NH/C=O groups of the urea linkages [26] and in $\bullet O–O–Si{\equiv}(CO_2)$ oxygen-related defects of the siliceous nanodomains [27]. The incorporation of lanthanide β-diketonate complexes into di-ureasils and di-urethanesils with short poly(ε-caprolactone) segments generally resulted in an enhancement in the emission quantum yield and emission quantum efficiency, relatively to those of the precursor complexes [17,28–30]. Furthermore, despite the continuous effort related to the photophysical characterization of lanthanide-based organic–inorganic hybrids, only recently comprehensive quantitative studies on the host-to-ligand

* Corresponding author. Tel.: +351 234 378110; fax: +351 234 378197.
E-mail address: patriciapereira@ua.pt (P.P. Lima).

1010-6030/$ – see front matter © 2008 Elsevier B.V. All rights reserved.
doi:10.1016/j.jphotochem.2008.10.021

and the host-to-metal energy transfer mechanisms have been reported [31,32].

Di-ureasils have been synthesized previously via conventional hydrolysis in the absence of catalyst [25] and carboxylic acid solvolysis [33,34]. The emission quantum yields of di-ureasils prepared by carboxylic acid solvolysis [33,34] are 27–35% higher than those determined for the di-ureasils synthesized via conventional hydrolysis. However, di-ureasils synthesized under ammonia atmosphere presented an emission quantum yield ($6.0 \pm 0.6\%$) close to that determined for di-ureasils prepared through conventional hydrolysis in the absence of catalyst [35]. Indeed, several catalysts have been used in the di-ureasil synthesis. For instance, ammonia and citric acid were employed by Boev et al. [36] whereas Chiavacci et al. [37] showed that the presence of HCl during the synthesis of iron-doped nanocomposites affects their structure, magnetic and thermomechanical properties and Molina et al. [38] used ammonium fluoride to catalyze the hydrolysis reaction of the alkoxy groups of Ti-based samples.

Herein, we report the synthesis and photoluminescence properties of di-ureasils (Scheme 1a) incorporating the $Tb(acac)_3{\cdot}3H_2O$ complex (Scheme 1b) prepared via conventional hydrolysis using HCl as catalyst. Four different concentrations of HCl were used (0.5, 1.0, 1.5 and 2.0 mol L^{-1}). For comparison purposes, one di-ureasil incorporating $Tb(acac)_3{\cdot}3H_2O$ complex was prepared via conventional hydrolysis in the absence of catalyst. For 1.5 mol L^{-1} HCl concentration, three different quantities of the $Tb(acac)_3{\cdot}3H_2O$ complex (0.01, 0.015 and 0.03 mmol) were incorporated into the di-ureasil host. The main objective of this work is to use HCl (0.5, 1.0, 1.5 and 2.0 mol L^{-1}) in order to decrease the gelation time (very fast, between 5 and 20 min, depending on the acid concentration), to improve the luminescent properties of the resulting hybrids, and to investigate the local Tb^{3+} environment in the different synthetic conditions.

2. Experimental

2.1. Synthesis

2.1.1. Synthesis of the $Tb(acac)_3{\cdot}3H_2O$ complex

The complex was prepared by an addition of terbium chloride ($TbCl_3{\cdot}6H_2O$, 99.9%, Aldrich) to acetyl acetone (99.5%, Aldrich) in an ethanol solution 1:3 molar ratio followed by the addition of sodium hydroxide until the pH reaches 6.5. The obtained complex was filtrated and dried under vacuum.

2.1.2. Synthesis of the hybrids

α, ω-diaminepoly(oxyethylene-co-oxypropylene) with a molecular weight of about 600 g mol^{-1}, corresponding to approximately 8.5 (OCH_2CH_2) repeat units and commercially designated as Jeffamine ED-600® (Fluka), was dried over molecular sieves (4 Å, 1.6 mm pellets, Aldrich) before use. The 3-isocyanatopropyltriethoxysilane precursor (ICPTES, Fluka, 95%) was used without further purification. Tetrahydrofuran (THF) and absolute ethanol were dried over molecular sieves at room temperature before use. The synthesis via conventional hydrolysis of the di-ureasils has already been described in detail elsewhere [25,33]. The first stage of the synthesis involves the reaction in THF of the isocyanate group of the alkoxysilane precursor ICPTES with the terminal amine groups of the doubly functional diamine to form a urea cross-linked organic–inorganic hybrid precursor, so-called d-UPTES(600) ureapropyltriethoxysilane. In the second step, the $Tb(acac)_3{\cdot}3H_2O$ complex was incorporated into the di-ureasil host.

Step 1: a volume of Jeffamine ED-600® (1.0 mL, 1.75 mmol) was dissolved in 5.0 mL of dried THF in a flask in a fume cupboard. A volume of ICPTES (0.91 mL, 3.5 mmol) was then added to this solution under stirring. The molar ratio of Jeffamine ED-600® to ICPTES was 1:2. The flask was sealed and the solution was stirred at room temperature in N_2 atmosphere for 24 h.

Step 2: a typical synthetic procedure is presented for the Tb^{3+}-based di-ureasils prepared with 0.5 mol L^{-1} HCl: 0.015 mmol of $Tb(acac)_3{\cdot}3H_2O$ complex was dissolved in ethanol, CH_3CH_2OH (0.82 mL, 14.04 mmol), and a volume of HCl (0.5 mol L^{-1}) (0.04 mL) was added to this solution. The acid character was observed in the solutions after addition of the HCl. The other samples were prepared according to this procedure varying the acid concentration (1.0, 1.5 and 2.0 mol L^{-1}) or complex amount. For the samples prepared with 1.5 mol L^{-1} HCl, three different quantities of $Tb(acac)_3{\cdot}3H_2O$ complex were incorporated into the di-ureasil (5.0 mg, 0.01 mmol; 7.6 mg, 0.015 mmol; 15.5 mg, 0.03 mmol). The molar ratio of ICPTES:CH_3CH_2OH is 1:4. Finally, the mixed solution was added to the precursor under stirring at room temperature. The undoped samples were obtained as transparent monoliths. The gelation time varied between 5 and 20 min at room temperature and the aging time was 7 days at 45 °C.

The hybrids are designated according to the acid concentration and the quantity of incorporated complex. The undoped hybrids prepared with 0.5, 1.0, 1.5 and 2 mol L^{-1} HCl are termed as d-U(600)-0.5M, d-U(600)-1M, d-U(600)-1.5M and d-U(600)-2M, respectively, whereas those incorporating $Tb(acac)_3{\cdot}3H_2O$ (0.015 mmol) prepared with 0.5, 1.0, 1.5, and 2 mol L^{-1} HCl are designated as d-U(600)-Tb15-0.5M, d-U(600)-Tb15-1M, d-U(600)-Tb15-1.5M and d-U(600)-Tb15-2M, respectively. The samples with 0.01 and 0.03 mmol of $Tb(acac)_3{\cdot}3H_2O$ prepared with 1.5 mol L^{-1} HCl are named as d-U(600)-Tb10-1.5M and d-U(600)-Tb30-1.5M, respectively, and finally the undoped and Tb^{3+}-based di-ureasils prepared by conventional hydrolysis in the absence of catalyst are designated as d-U(600) and d-U(600)-Tb15, respectively.

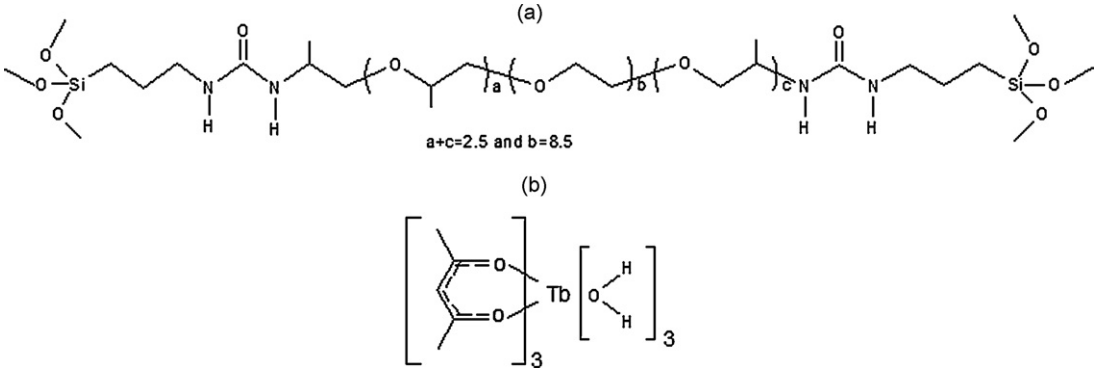

Scheme 1. Chemical structures of (a) the di-ureasil organic–inorganic hybrid and the (b) $Tb(acac)_3{\cdot}3H_2O$ complex.

2.2. Instrumentation

2.2.1. Powder X-ray diffraction (XRD)

X-ray diffraction patterns were recorded using a Philips X'Pert MPD Powder X-ray diffractometer system. The powders were exposed to the Cu Kα radiation (λ = 1.54 Å) at room temperature in a 2θ range (scattering angle) between 1 and 70°. The xerogel samples, analyzed as films, were not submitted to any thermal pretreatment.

2.2.2. Nuclear magnetic resonance (NMR)

^{29}Si magic-angle spinning (MAS) and ^{13}C cross-polarization (CP) MAS NMR spectra were recorded on a Bruker Avance 400 (9.4 T) spectrometer at 79.49 and 100.62 MHz, respectively. ^{29}Si MAS NMR spectra were recorded with 2 μs (equivalent to 30°) rf pulses, a recycle delay of 60 s and at a 5.0-kHz spinning rate. ^{13}C CP/MAS NMR spectra were recorded with 4 μs ^{1}H 90° pulse, 2 ms contact time, a recycle delay of 4 s and at a spinning rate of 8 kHz. Chemical shifts are quoted in ppm from tetramethyl silane (TMS).

2.2.3. Fourier transform infrared spectroscopy (FTIR)

FTIR spectra were recorded at room temperature using a MATTSON 7000 FTIR spectrometer. The spectra were collected over the range 4000–400 cm^{-1} by averaging 128 scans at a maximum resolution of 4 cm^{-1}. The hybrids were finely ground (about 2 mg), mixed with approximately 175 mg of dried potassium bromide (Merck, spectroscopic grade) and pressed into pellets. Consecutive spectra were recorded until reproducible results were obtained. To evaluate complex band envelopes and to identify underlying component bands of the spectra, the interactive least-squares curve-fitting procedure in Peakfit® [39] software was used extensively throughout this study. The best fit of the experimental data was sought by varying the frequency, bandwidth, and intensity of the bands and by employing Voigt band shapes (a mixture of Lorentzian and Gaussian contributions). A linear baseline correction with a tolerance of 0.2% was employed. The stand errors of the curve-fitting procedure were less than 0.003.

2.2.4. Photoluminescence

The photoluminescence spectra were recorded at room temperature with a modular double grating excitation spectrofluorimeter with a TRIAX 320 emission monochromator (Fluorolog-3, Jobin Yvon-Spex) coupled to a R928 Hamamatsu photomultiplier, using the front face acquisition mode. The excitation source is a 450-W Xe arc lamp. The emission spectra were corrected for detection and optical spectral response of the spectrofluorimeter and the excitation spectra were corrected for the spectral distribution of the lamp intensity using a photodiode reference detector. The room temperature lifetime measurements were acquired with the setup described for the luminescence spectra using a pulsed Xe–Hg lamp (6 μs pulse at half width and 20–30 μs tail).

2.2.5. Emission quantum yields

The absolute emission quantum yield was measured at room temperature using the technique for powered samples described by Brill and De Jager-Veenis [40,41]. The emission quantum yield, q_x, defined as the ratio between the number of emitted and absorbed photons, were determined according to:

$$q_x = \left(\frac{1 - r_{st}}{1 - r_x}\right)\left(\frac{\Delta\Phi_x}{\Delta\Phi_{st}}\right) q_{st} \quad (1)$$

where r_{st} and r_x are the amounts of reflected radiation by the standard phosphor and by the sample, respectively, and q_{st} is the quantum yield of the standard phosphor. The values of r_{st}, r_x, $\Delta\Phi_x$ and $\Delta\Phi_{st}$ must be obtained for the same excitation wavelength, geometry and experimental conditions. The terms $\Delta\Phi_x$ and $\Delta\Phi_{st}$ give the integrated photon flux (photons s^{-1}) for the sample and the standard phosphor (sodium salicylate, Merck PA), respectively. In order to have absolute values for the reflected radiation, $BaSO_4$ is used as reflectance standards (r = 91%) [42]. A detailed description of this method has been presented elsewhere [43,44]. The errors in the quantum yields values associated with this technique were estimated within 10% [40].

The emission quantum yields for the Tb^{3+}-based di-ureasils were measured using the commercial C9920-02 system from Hamamatsu with a 150-W Xe lamp coupled to a monochromator for wavelength discrimination, an integrating sphere as sample chamber and a multichannel analyzer for signal detection. The errors in the quantum yields values associated with this technique were estimated within 5%.

3. Results and discussion

3.1. Powder X-ray diffraction

The XRD patterns of d-U(600)-0.5M, d-U(600)-1M and d-U(600)-2M are shown in Fig. 1a. All the diffractograms exhibit a peak centered at approximately 21.6° indicating the presence of ordering within the siliceous domains [33,34]. The second-order of this peak appears as a broad weak hump around 35–48°. The structural units distances, calculated using the Bragg law, are approximately 4.01–4.19 Å. The coherence lengths, L, have been estimated using the modified Scherrer equation $L = I\lambda/(A\cos\theta)$, where I and A, in radians, are the maximum intensity and integrated area of the first sharp diffraction peak, respectively, and λ is the wavelength of the incident radiation. The L values obtained for the undoped samples lie between 14.59 and 15.05 Å. From the peak maximum position we can estimate an average interparticle distance between 21.8 and 25.2 ± 2 Å. These structural units values are similar to those obtained for undoped di-ureasils prepared via conventional hydrolysis in the absence of catalyst or carboxylic acid solvolysis [33,34], indicating that the HCl catalyst does not alter the hybrids local structure.

Fig. 1b shows the diffractograms of d-U(600)-Tb15-0.5M, d-U(600)-Tb15-1.5M and d-U(600)-Tb15-2M. The peak that indicates the presence of ordering within the siliceous domain is centered at approximately 21.3° and the calculated L values ranges between 13.73 and 16.49 Å. The peak appearing at lower angles, between 3.5 and 4.0 Å (insets in Fig. 1a and b), has been assigned to an interparticle scattering interference [33,34]. From the analysis of the XRD patterns of Fig. 1b we can conclude that the $Tb(acac)_3{\cdot}3H_2O$ incorporation into the di-ureasil host does not significantly altered the hybrid's local structure.

3.2. Nuclear magnetic resonance

The ^{29}Si MAS NMR spectra of d-U(600)-0.5M, d-U(600)-1M, d-U(600)-1.5M and d-U(600)-2M are shown in Fig. 2a. These spectra exhibit broad signals characteristic of T_1, T_2 and T_3 units [26]. The absence of T_0 signal indicates that unreacted precursor is absent. The calculated condensation degree c, $c = 1/3\,(\%T_1 + 2\%T_2 + 3\%T_3)$, of d-U(600)-0.5M, d-U(600)-1M, d-U(600)-1.5M, and d-U(600)-2M, are 76, 83, 78 and 81%, respectively, values much lower than those of undoped di-ureasils prepared via acetic acid solvolysis and conventional hydrolysis [33,34], although similar to those found in other sol–gel derived acid catalysis hybrids [45,46]. The acid catalysis leads to more polymeric forms of the gel with linear chains as intermediates, leading to lower values for the condensation degree [21].

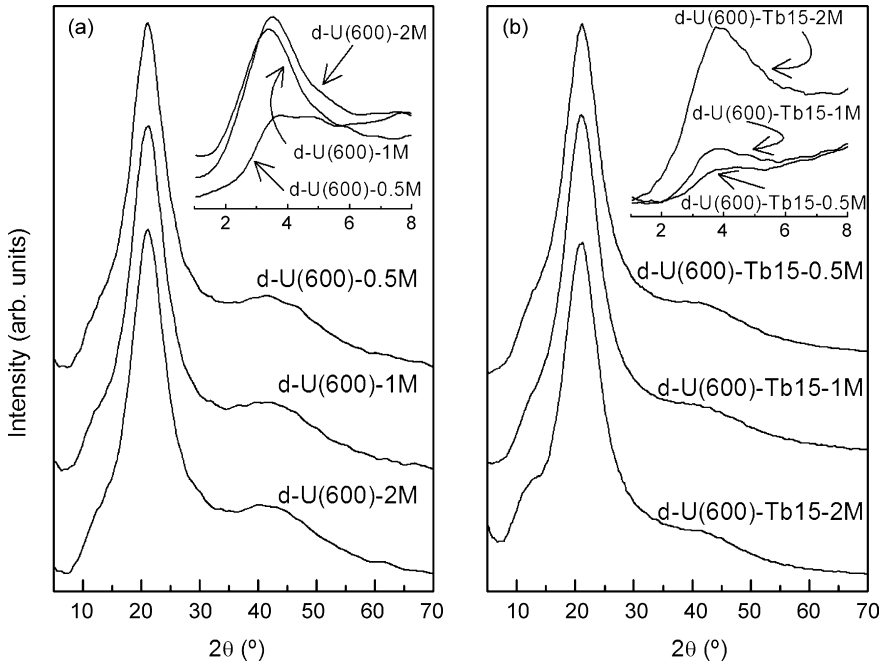

Fig. 1. (a) XRD patterns of d-U(600)-0.5M, d-U(600)-1M, and d-(600)-2M. (b) XRD patterns of d-U(600)-Tb15-0.5M, d-U(600)-Tb15-1M, and d-U(600)-Tb15-2M.

The ^{13}C CP MAS NMR spectra of the undoped samples prepared with HCl (Fig. 2b) resemble closely those reported for d-U(600) prepared via conventional hydrolysis or carboxylic acid solvolysis [33,34]. The peak at 70.5 ppm is attributed to –(OCH_2CH_2)– whereas the shoulder at about 75.2 ppm is originated from the main-chain carbons of propylene oxide. The peaks at 45 and 24 ppm are characteristics of the $(CH_2)_3$ aliphatic chains and the very weak peak at approximately 159 ppm is associated with the C=O groups of the urea-linkages. The signal at 18.7 ppm is assigned to different $–CH_3$ groups of the polymer chains, while the shoulder at 17.4 ppm is ascribed to the carbons ethoxy groups. The spectra of the doped hybrids (not shown) exhibit similar profiles compared with those of the undoped di-ureasils synthesized via conventional hydrolysis or carboxylic acid solvolysis.

3.3. Fourier transform infrared spectroscopy

The FTIR spectra show small differences between the undoped samples prepared with and without HCl, namely in the "amide I" region (Fig. 3). The "amide I" mode is a highly complex vibration involving the contribution of the C=O stretching, the CN stretching and the C–C–N deformation [33]. Fig. 3a–c shows the

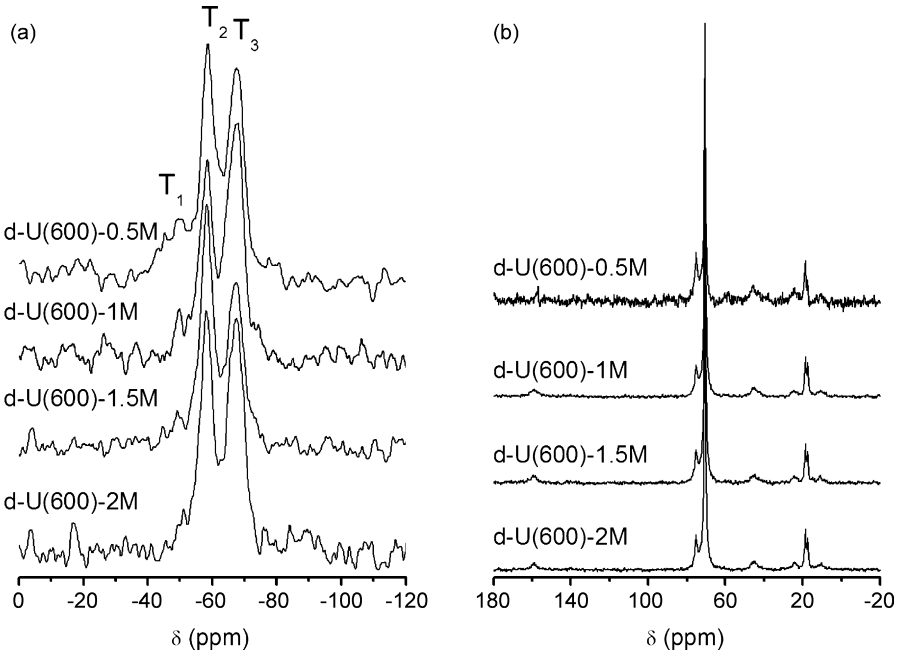

Fig. 2. (a) ^{29}Si MAS NMR spectra of d-U(600)-0.5M, d-U(600)-1M, d-U(600)-1.5M, and (d) d-(600)-2M. (b) ^{13}C MAS NMR spectra of d-U(600)-0.5M, d-U(600)-1M, d-U(600)-1.5M and (d) d-(600)-2M.

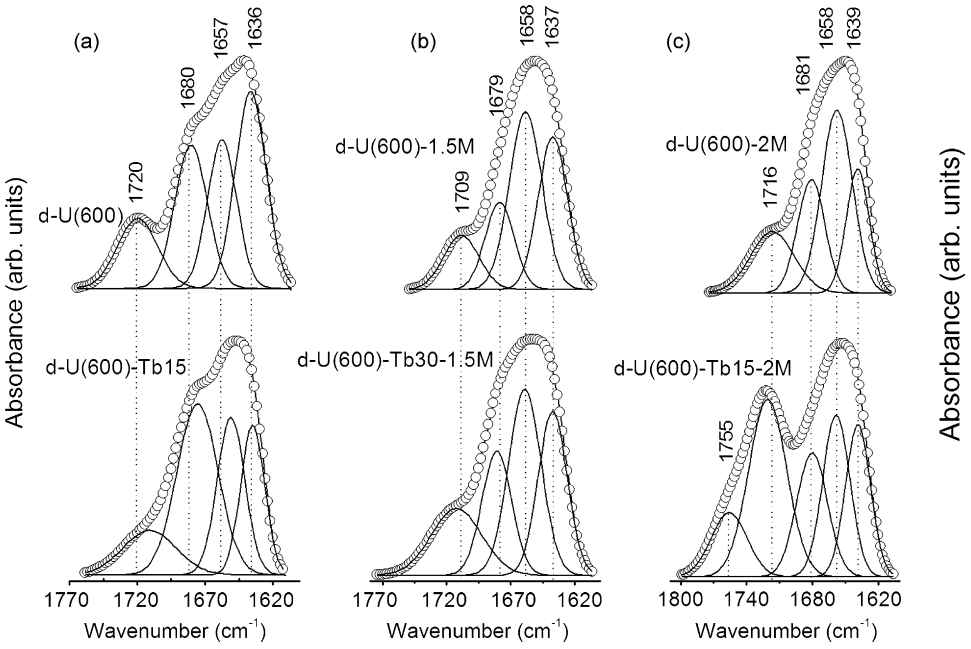

Fig. 3. Results of curve-fitting performed in the "amide I" region of FTIR spectra of (a) d-U(600) and d-U(600)-Tb15, (b) d-U(600)-1.5M and d-U(600)-Tb30-1.5M, and (c) d-U(600)-2M and d-U(600)-Tb30-2M. The frequencies indicated represent the average value of the frequencies of the samples considered in each case.

curve-fitting performed in that region for d-U(600), d-U(600)-1.5M and d-U(600)-2M, respectively. The spectra of d-U(600)-0.5M and d-U(600)-1M were omitted because they resemble that of Fig. 3b. For the undoped samples the "amide I" was resolved into four components at approximately 1709, 1678, 1657 and 1637 cm^{-1}, accordingly to the literature [34]. The first three components are ascribed to C=O groups belonging to disordered hydrogen-bonded POE/urea associations of increasing strength while the last feature is assigned to C=O groups included in significantly more ordered hydrogen bonded urea–urea associations [34]. The absence of the 1750 cm^{-1} component indicates that all the urea groups are involved in hydrogen bonding interactions [25]. The analysis of the integral area fraction of the four components revealed that the fraction around 1713 cm^{-1} increase from 6.71% for d-U(600)-0.5M to 18.75% for d-U(600)-2M. However, the fraction around 1637 cm^{-1} decreases from 29.24% for d-U(600)-0.5M to 19.84% for d-U(600)-2M. This indicates that the urea–urea fraction is progressively disrupted with the increase of the HCl concentration.

The incorporation of $Tb(acac)_3{\cdot}3H_2O$ into the hybrid matrix, despite the low Tb^{3+} concentration (0.5–1%), disturbs the "amide I" region leading to a band redistribution (Fig. 3a–c). An increase in the 1680 cm^{-1} component and a decrease in that around 1637 cm^{-1} are observed suggesting the Tb^{3+} coordination to the oxygen atoms of the carbonyl group of the urea cross-linkages. The component at 1755 cm^{-1} for the d-U(600)-Tb15-2M indicates the presence of free urea groups (not involving in urea-urea hydrogen bonded arrays) [25]. Especially for d-U(600)-Tb15-2M we suggest that the presence of 2 mol L^{-1} HCl may favors the protonation of the acac ligands and therefore the complex may lost at least one of its acac ligands that will disrupt the urea–urea hydrogen bonded array with the subsequent appearance of free urea moieties. We will return to this point later.

3.4. Photoluminescence measurements

Fig. 4 shows the emission spectra of d-U(600)-1.5M which is similar to those of d-U(600)-0.5M, d-U(600)-1M and d-U(600)-2M. The spectra consist of a broad band between 340 and 630 nm, whose maximum emission energy shifts towards the red as excitation wavelength increases. This large broad band has already been observed in similar organic–inorganic hybrids prepared by conventional hydrolysis and carboxylic acid solvolysis [26,27,33,34,47] being ascribed to the convolution of donor–acceptor pair recombinations that occur in the NH/C=O groups of the urea linkages and in the siliceous nanodomains [27].

Similar to the di-ureasils prepared via conventional hydrolysis or carboxylic acid solvolysis, the excitation spectra of the d-U(600)-1.5M (inset in Fig. 4) is formed of a broad band between 280 and 470 nm. As the monitoring energy decreases, the maximum intensity of the excitation band is redshifted and the band becomes broader suggesting the presence of two components. As pointed out elsewhere, the higher and lower energetic sides of the excitation spectra can be ascribed to the preferential excitation of the emission originated in the siliceous and NH groups, respectively [33,34].

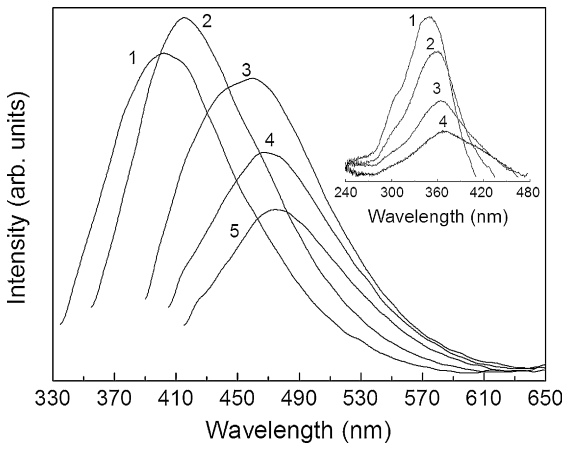

Fig. 4. Room-temperature emission spectra of d-U(600)-1.5M. The excitation wavelengths are (1) 320, (2) 340, (3) 375, (4) 390, and (5) 400 nm. The inset shows the room-temperature excitation spectra of d-U(600)-1.5M monitored at (1) 425, (2) 450, (3) 480 and (4) 500 nm.

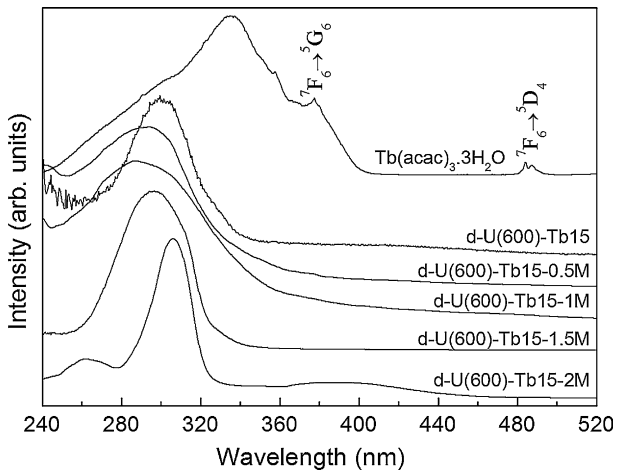

Fig. 5. Room-temperature excitation spectra of Tb(acac)$_3$·3H$_2$O, d-U(600)-Tb15, d-U(600)-Tb-0.5M, d-U(600)-Tb-1M, d-U(600)-Tb15-1.5M, and d-U(600)-Tb-2M monitored between 542 and 548 nm.

Fig. 5 shows the excitation spectra of Tb(acac)$_3$·3H$_2$O, d-U(600)-Tb15, d-U(600)-Tb15-0.5M, d-U(600)-Tb15-1.5M, and d-U(600)-Tb15-2M monitored within the $^5D_4 \rightarrow {}^7F_5$ emission line. The spectrum of the complex is formed of a large broad band (structured with three components, at least, centered at 300, 335 and 370 nm), related to the ligand triplet excited states and a series of Tb^{3+} intra-4f^8 transitions. The excitation spectrum of d-U(600)-Tb-2M also presents a large broad band of low relative intensity between 350 and 490 nm ascribed to the hybrid host excited states.

The intensity of the ligand excited states (maximum at 370 nm) in the excitation spectra of the hybrids is significantly reduced, relatively to that of Tb(acac)$_3$·3H$_2$O, readily pointing out a effective interaction between the hybrid host and the Tb^{3+} ions. This is also supported by the absence of the intra-4f^8 transitions in the excitation spectra of the hybrids indicating that the Tb^{3+} ions are mainly excited via an effective sensitized process involving the ligand excited states, rather than by direct intra-4f^8 excitation. Furthermore, the substantially decrease of the full width at half maximum (*fwhm*) of the ligands broad band for the d-U(600)-Tb15-2M hybrid may be in agreement with the mentioned above modifications in the Tb^{3+} local coordination induced by acac protonation.

The emission spectra for Tb(acac)$_3$·3H$_2$O, d-U(600)-Tb15, and d-U(600)-Tb15-1.5M (Fig. 6) display the intra-4f^8 $^5D_4 \rightarrow {}^7F_{6-0}$ lines and an emission broad band in the blue-green spectral region, already observed for the undoped hybrids (Fig. 4). For the Tb^{3+}-based di-ureasils prepared with 1.5 mol L^{-1} HCl such emission broad band presents a relatively low intensity (Fig. 6), indicating an efficient energy transfer process from the hybrid emitting centers to Tb^{3+} complex, as already suggested in the excitation spectra.

With the aim to infer from possible changes in the Tb^{3+} first coordination sphere induced by the incorporation of the complex into the di-ureasil host and the different synthetic conditions used, Fig. 7 compares the $^5D_4 \rightarrow {}^7F_{6-3}$ emission lines for the Tb(acac)$_3$·3H$_2$O complex and Tb^{3+}-based di-ureasils. Changes are observed in the energy, number of Stark components, and *fwhm* re-enforcing the Tb^{3+}-hybrid host interaction mentioned previously. The increase of the *fwhm* of the intra-4f^8 transitions in the emission spectra of the hybrids, relatively to that of the complex (approximately between 1.3 and 2 times) points out a higher non-homogeneous distribution of Tb^{3+} chemical environments due to changes outside the coordination polyhedron [30]. Concerning the influence of the HCl concentration, the spectrum of the d-U(600)-Tb15-2M di-ureasil displays marked differences relatively to those of the other hybrids, *e.g.* an inversion in the intensity ratio of the two main lines of the $^5D_4 \rightarrow {}^7F_5$ transition and a new Stark component in the $^5D_4 \rightarrow {}^7F_{6,4}$ lines (Fig. 7). These findings reinforce the fact that for d-U(600)-Tb15-2M the Tb^{3+} local environment is strongly modified probably due to acac protonation with the consequent replacement of acac ligands by the carbonyl groups of the di-ureasil host.

The room temperature $^5D_4$ lifetimes were monitored around the more intense emission transition ($^5D_4 \rightarrow {}^4F_5$) and the decay curves are well described by a single exponential, indicating a single Tb^{3+} local coordination site. For all the di-ureasils the lifetime values are larger than that of the Tb(acac)$_3$·3H$_2$O complex (0.774 ± 0.001 ms), suggesting that the water molecules of the first coordination sphere were replaced by the carbonyl group of the hybrid host. Fig. 8 shows the $^5D_4$ lifetime values as a function of the HCl concentration. For the Tb^{3+}-based di-ureasils prepared with 1.5 mol L^{-1} HCl (the HCl concentration that corresponds to the greater lifetime value), the $^5D_4$ lifetime decreases with the increase of the Tb^{3+} concentration (1.337, 1.329 and 1.040 ms for 0.01, 0.015 and 0.030 mmol, respectively). A similar behavior reported for Tb(acac)$_3$·4H$_2$O incorporated into diglycidyl epoxy resin [48] was also explained assuming that the water molecules of the complex were replaced by the oxirane polymer ring of the polymer.

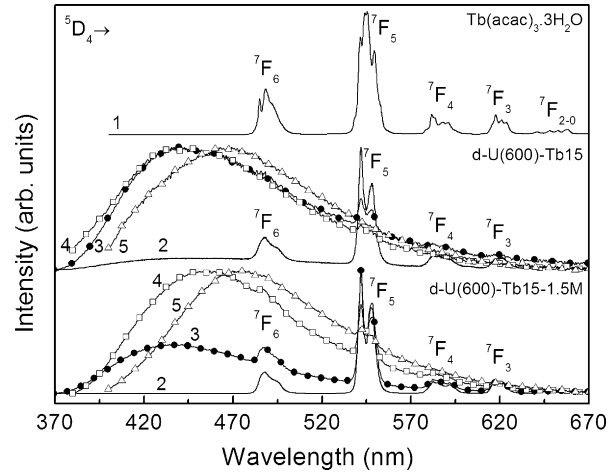

Fig. 6. Room-temperature emission spectra of Tb(acac)$_3$·3H$_2$O, d-U(600)-Tb15 and d-U(600)-Tb15-1.5M. The excitation wavelengths are (1) 333, (2) 300, (3) 340, (4) 360, and (5) 385 nm.

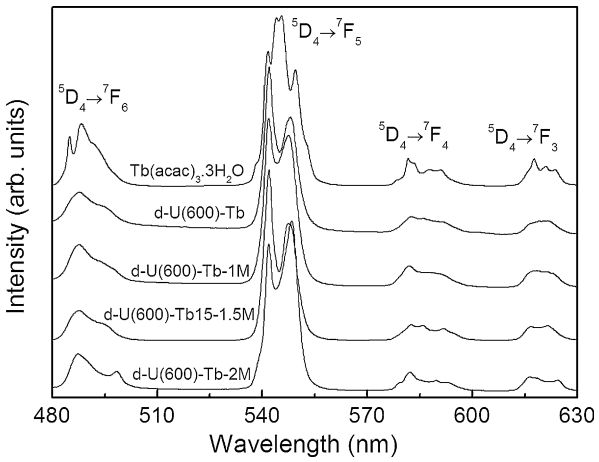

Fig. 7. Room-temperature emission spectra of the $^5D_4 \rightarrow {}^7F_{6-3}$ transitions for Tb(acac)$_3$·3H$_2$O, d-U(600)-Tb15, d-U(600)-Tb15-0.5M, d-U(600)-Tb15-1.5M, and d-U(600)-Tb15-2M.

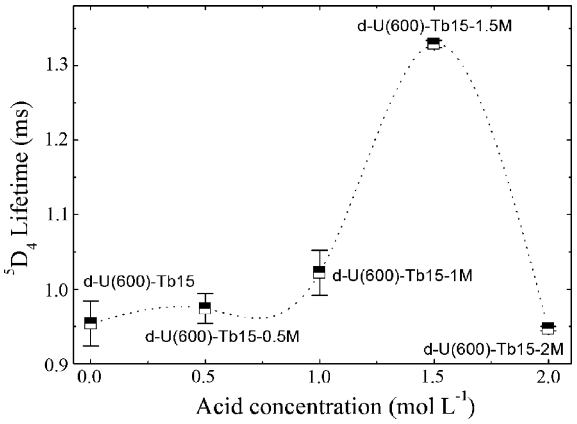

Fig. 8. $^5D_4$ lifetime as a function of the HCl concentration used in the synthesis of the Tb^{3+}-based di-ureasils. The line is a guide for the eyes.

3.5. Emission quantum yields and color coordinates

The emission quantum yield values for d-U(600)-0.5M, d-U(600)-1M, d-U(600)-1.5M, and d-U(600)-2M, measured at an excitation wavelength of 360 nm, are 8.7, 9.5, 10.6 and 9.4%, respectively. These values are similar to those obtained for d-U(600) samples prepared by carboxylic acid solvolysis (9.6–10.4%), are higher than those measured for samples synthesized via conventional hydrolysis (6.6%).

Fig. 9a shows the emission quantum yield as a function of the excitation wavelength (300–380 nm) for d-U(600)-Tb15, d-U(600)-Tb15-1M, d-U(600)-Tb15-1.5M and d-U(600)-Tb30-1.5M. For all the samples an increase in the emission quantum yield is discerned for excitation wavelengths between 350 and 380 nm that corresponds to the preferential excitation of the hybrid broad band emission (Fig. 6). This is illustrated in Fig. 9b that displays the excitation spectra of the d-U(600)-Tb15-1M hybrid. The dependence of the emission quantum yield with the concentration of the catalyst and with the Tb^{3+} amount, maximum values measured, respectively, for d-U(600)-Tb15-1M and d-U(600)-Tb30-1.5M, is presently inexplicable warranting further studies.

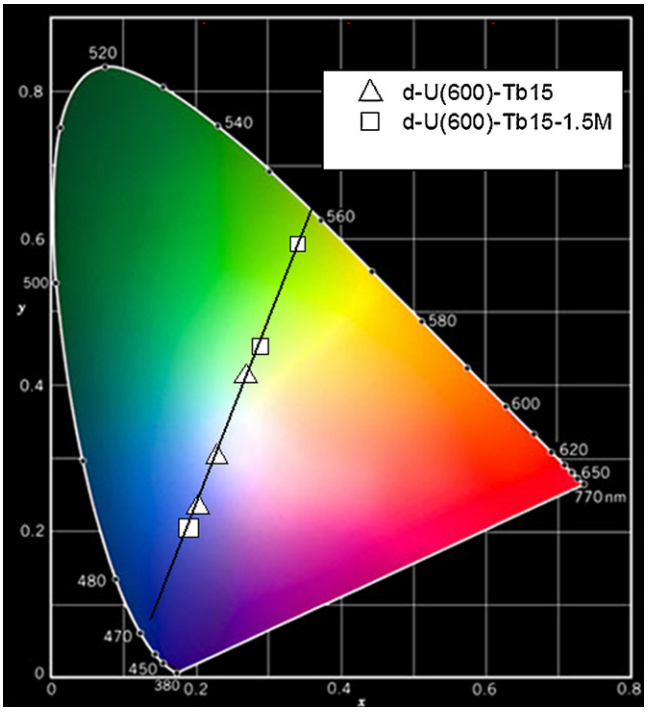

Fig. 10. Partial 1931 CIE (*x*,*y*) diagram displaying emission color coordinates of d-U(600)-Tb15 and d-U(600)-Tb15-1.5M excited at (1) 300 nm, (2) 320 nm and (3) 360 nm (room temperature).

The emission features were also quantified for the d-U(600)-Tb15 and d-U(600)-Tb30-1.5M hybrids through the measurement of the (*x*,*y*) chromaticity coordinates, according to the standard procedure defined by the Commission Internacionale d'Eclairage (CIE) (Fig. 10). Clearly the different synthesis conditions affected the emission color coordinates. For the Tb^{3+}-based di-ureasil prepared without HCl the emission colors coordinates change within the white–blue region from (0.257, 0.399) to (0.191, 0.218), while for the sample prepared with 1.5 mol L^{-1} HCl the color changes within the green–blue region from (0.330, 0.582) to (0.179, 0.189).

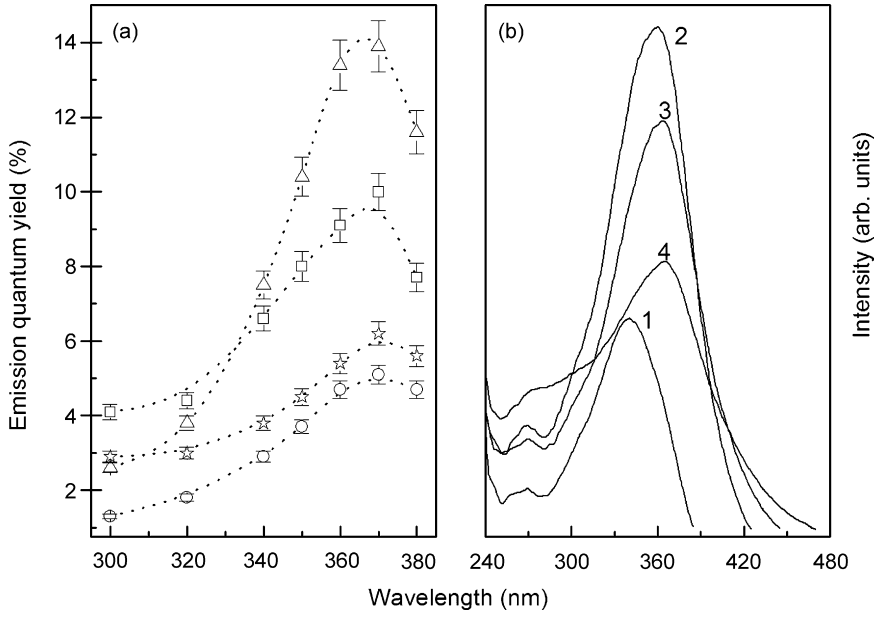

Fig. 9. (a) Emission quantum yield as a function of the excitation wavelength (300–380 nm) for (open circles) d-U(600)-Tb15, (open triangles) d-U(600)-Tb15-1M, (open stars) d-U(600)-Tb15-1.5M, and (open squares) d-U(600)-Tb30-1.5M. (b) Excitation spectra of d-U(600)-Tb15-1M monitored at (1) 400, (2) 440, (3) 460 and (4) 485 nm.

4. Conclusions

In this work the $Tb(acac)_3{\cdot}3H_2O$ complex was incorporated into the di-ureasil hybrid host via conventional hydrolysis sol–gel reactions in the presence and absence of an acid catalyst, HCl (0.5, 1.0, 1.5 and 2.0 mol L^{-1}). Undoped samples were also prepared using these same HCl concentrations. The acid catalyst contributes in the decrease of the gelation time for all samples. Depending on the HCl concentration gelation occurs between five and twenty minutes. The structural data obtained reveal that, independently of the HCl concentration used, the undoped di-ureasils are structurally similar to materials prepared via the conventional sol–gel route in the absence of catalyst.

For the Tb^{3+}-based di-ureasils an increase in the $^5D_4$ lifetime, in comparison with that of the $Tb(acac)_3{\cdot}3H_2O$ complex, suggests that the coordination ability of the hybrid host is strong enough to replace water molecules from the Tb^{3+} first coordination sphere by carbonyl groups of the urea moieties, a conclusion supported by the analysis of the "amide I" region of the infrared spectra of the Tb^{3+}-based di-ureasils. The emission quantum yields measured for the undoped samples (between 8.7 and 10.6%) although similar to those of the d-U(600) hybrids prepared by carboxylic acid solvolysis, are higher than those obtained by conventional hydrolysis (in fact the value for d-U(600)-1.5M is the highest one reported for the d-U(600) host). All the Tb^{3+}-based di-ureasils prepared with HCl present the emission quantum yield and lifetime higher than that prepared without HCl. From the emission spectra of the Tb^{3+}-based di-ureasils changes were observed in the energy and *fwhm* of the intra-$4f^8$ lines indicating that the different synthetic conditions used to prepare these materials affected indeed the Tb^{3+} local coordination. Particularly for d-U(600)-Tb15-2M the profile of the excitation spectrum, the energy and the *fwhm* of the $^5D_4 \rightarrow {}^7F_{6\text{-}3}$ transitions suggest that the $Tb(acac)_3{\cdot}3H_2O$ lost one or more of its acac ligands after incorporation into the di-ureasil host. The emission color varies along the chromaticity diagram from the blue to the green spectral regions crossing the white area and this is achieved either by changing the HCl or Tb^{3+} concentration, or the excitation wavelength.

Acknowledgments

This work was supported by Fundação para a Ciência e Tecnologia (SFRH/BPD/34365/2006), CAPES and CNPq (Brazilian agencies) and the RENAMI project (Brazilian Molecular and Interfaces Nanotechnology Network). The authors would like to thank Dr. Verónica Zea Bermudez (UTAD, Portugal) and Prof. João Rocha (University of Aveiro, Portugal) for their help on the infrared spectra and on the $^{29}Si/^{13}C$ NMR measurements, respectively.

References

[1] S. Capecchi, O. Renault, D.G. Moon, M. Halim, M. Etchells, P.J. Dobson, O.V. Salata, V. Chrisou, Adv. Mater. 12 (2000) 1591.
[2] Y. Zheng, J. Lin, Y. Liang, Q. Lin, Y. Yu, Q. Meng, Y. Zhou, S. Wang, H. Wang, H. Zhang, J. Mater. Chem. 11 (2001) 2615.
[3] R. Reyes, M. Cremona, E.E.S. Teotonio, H.F. Brito, O.L. Malta, Chem. Phys. Lett. 396 (2004) 54.
[4] W.G. Quirino, C. Legnani, M. Cremona, P.P. Lima, S.A. Junior, O.L. Malta, Thin Solid Films 494 (2006) 23.
[5] T. Oyamada, Y. Kawamura, T. Koyama, H. Sasabe, C. Adachi, Adv. Mater. 16 (2004) 1082.
[6] D. Parker, P. Kanthi-Senanayake, J.A.G. Williams, J. Chem. Soc., Perkin Trans. 2 (1998) 2129.
[7] C.M.G. dos Santos, P.B. Fernandez, S.E. Plush, J.P. Leonard, T. Gunnlaugsson, Chem. Commun. 32 (2007) 3389.
[8] C.G. Gameiro, E.F. da Silva Jr., S. Alves Jr., G.F. de Sá, P.A. Santa-Cruz, J. Alloys Comp. 323–324 (2001) 820.
[9] C.G. Gameiro, C.A. Achete, R.A. Simão, E.F. da Silva Jr., P.A. Santa-Cruz, J. Alloys Comp. 344 (2002) 385.
[10] K. Binnemans, in: K.A. Gschneider Jr., J.C.G. Bunzli, V.K. Pecharsky (Eds.), Handbook on the Physics and Chemistry of Rare Earths, 35, Elsevier, Amsterdam, 2005, pp. 107–272 (Chapter 225).
[11] S. Biju, D.B. Ambili Raj, M.L.P. Reddy, B.M. Kariuki, Inorg. Chem. 45 (2006) 10651.
[12] H.J. Batista, A.V.M. de Andrade, R.L. Longo, A.M. Simas, G.F. de Sá, N.K. Ito, L.C. Thompson, Inorg. Chem. 37 (1998) 3542.
[13] H.F. Brito, O.L. Malta, J.F.S. Menezes, J. Alloys Comp. 303–304 (2000) 336.
[14] R. Bonzanini, D.T. Dias, E.M. Girotto, E.C. Muniz, M.L. Baesso, J.M.A. Caiut, Y. Messaddeq, S.J.L. Ribeiro, A.C. Bento, A.F. Rubira, J. Lumin. 117 (2006) 61.
[15] D.F. Parra, A. Mucciolo, D.G. Duarte, H.F. Brito, A.B. Lugão, J. Appl. Polym. Sci. 100 (2006) 406.
[16] D.F. Parra, A. Mucciolo, H.F. Brito, L.C. Thompson, J. Solid State Chem. 171 (2003) 412.
[17] M. Fernandes, V. de Zea Bermudez, R.A.S. Ferreira, L.D. Carlos, A. Charas, J. Morgado, M.M. Silva, M.J. Smith, Chem. Mater. 19 (2007) 3892.
[18] (a) Q.M. Wang, B. Yan, J. Mater. Chem. 14 (2004) 2450;
(b) Q.M. Wang, B. Yan, Crystal Growth Des. 5 (2005) 497;
(c) B. Yan, F.F. Wang, J. Organometal. Chem. 12 (2007) 2395.
[19] D. Zhao, S.-J. Seo, B.-S. Bae, Adv. Mater. 19 (2007) 3473.
[20] (a) K. Binnemans, P. Lenaerts, K. Driesen, C. Görller-Walrand, J. Mater. Chem. 14 (2004) 191;
(b) P. Lenaerts, C. Görller-Walrand, K. Binnemans, J. Lumin. 117 (2006) 163.
[21] H.D. Gesser, P.C. Goswami, Chem. Rev. 89 (1989) 765.
[22] L.L. Hench, J.K. West, Chem. Rev. 90 (1990) 33.
[23] C. Sanchez, G.J. de A.A. Soler-Illia, F. Ribot, T. Lalot, C.R. Mayer, V. Cabuil, Chem. Mater. 13 (2001) 3061.
[24] C. Sanchez, G.J. De, A.A. Soler-Illia, F. Ribot, D. Grosso, C. R. Chim. 6 (2003) 1131.
[25] V. de Zea Bermudez, L.D. Carlos, L. Alcácer, Chem. Mater. 11 (1999) 569.
[26] L.D. Carlos, R.A.S. Ferreira, V. De Zea Bermudez, S.J.L. Ribeiro, Adv. Funct. Mater. 11 (2001) 111.
[27] L.D. Carlos, R.A.S. Ferreira, R.N. Pereira, M. Assunção, V. de Zea Bermudez, J. Phys. Chem. B 108 (2004) 14924.
[28] R. Moleski, E. Stathatos, V. Bekiari, P. Lianos, Thin Solid Films 416 (2002) 279.
[29] C. Molina, K. Dahmouche, Y. Messaddeq, S.J.L. Ribeiro, M.A.P. Silva, V. de Zea Bermudez, L.D. Carlos, J. Lumin. 104 (2003) 93.
[30] P.P. Lima, R.A.S. Ferreira, R.O. Freire, F.A.A. Paz, L. Fu, S.A. Júnior, L.D. Carlos, O.L. Malta, Chem. Phys. Chem. 7 (2006) 735.
[31] S.S. Nobre, P.P. Lima, L. Mafra, R.A.S. Ferreira, R.O. Freire, L. Fu, U. Pischel, V. de Zea Bermudez, O.L. Malta, L.D. Carlos, J. Phys. Chem. C 111 (2007) 3275.
[32] P.P. Lima, S.S. Nobre, R.O. Freire, S.A. Junior, R.A.S. Ferreira, U. Pischel, O.L. Malta, L.D. Carlos, J. Phys. Chem. C 111 (2007) 17627.
[33] L.S. Fu, R.A.S. Ferreira, N.J.O. Silva, L.D. Carlos, V. de Zea Bermudez, J. Rocha, Chem. Mater. 16 (2004) 1507.
[34] L.S. Fu, R.A.S. Ferreira, M. Fernandes, S.C. Nunes, V. de Zea Bermudez, G. Hungerford, J. Rocha, L.D. Carlos, Opt. Mater. 30 (2008) 1058.
[35] M.C. Neves, M.A. Martins, P.C.R. Soares-Santos, P. Rauwel, R.A.S. Ferreira, T. Monteiro, L.D. Carlos, T. Trindade, Nanotechnology 19 (2008) 155601.
[36] V.I. Boev, A. Soloviev, C.J.R. Silva, M.J.M. Gomes, D.J. Barber, J. Sol–Gel Sci. Technol. 41 (2007) 223.
[37] L.A. Chiavacci, K. Dahmouche, N.J.O. Silva, L.D. Carlos, V.S. Amaral, V. de Zea Bermudez, S.H. Pulcinelli, C.V. Santilli, V. Briois, A.F. Craievich, J. Non-Cryst. Solids 345–346 (2004) 585.
[38] C. Molina, K. Dahmouche, P. Hammer, V. de Zea Bermudez, L.D. Carlos, M. Ferrari, M. Montagna, R.R. Gonçalves, L.F.C. de Oliveira, H.G.M. Edwards, Y. Messaddeq, S.J.L. Ribeiro, J. Braz. Chem. Soc. 17 (2006) 443.
[39] Peak Fit is a product of Jandel Corporation, 2591 Rerner Boulervard, San Rafael, CA 94901, USA.
[40] A. Bril, A.W. De Jager-Veenis, J. Electrochem. Soc. 123 (1976) 396.
[41] A.W. De Jager-Veenis, A. Bril, Philips J. Res. 33 (1978) 124.
[42] G.F. de Sá, O.L. Malta, C. de Mello Donegá, A.M. Simas, R.L. Longo, P.A. Santa-Cruz, E.F. Silva Jr., Coord. Chem. Rev. 196 (2000) 165.
[43] C. de Mello Donega, S. Alves Jr., G.F. de Sá, Chem. Commun. 10 (1996) 1199.
[44] C. de Mello Donegá, S.J.L. Ribeiro, R.R. Gonçalves, G. Blasse, J. Phys. Chem. Solids 57 (1996 1727).
[45] A.-C. Franville, R. Mahiou, D. Zambon, J.-C. Cousseins, Sol. State Sci. 3 (2001) 211.
[46] S.S. Nobre, C.D.S. Brites, R.A.S. Ferreira, V. de Zea Bermudez, C. Carcel, J.J. Moreau, J. Rocha, M.W. Chi Man, L.D. Carlos, J. Mater. Chem. 18 (2008) 4172.
[47] T. Brankova, V. Bekiari, P. Lianos, Chem. Mater. 15 (2003) 1855.
[48] D.F. Parra, A. Mucciolo, H.F. Brito, J. Appl. Polym. Sci. 94 (2004) 865.